NANO LETTERS
Letter
Cite This: Nano Lett. XXXX, XXX, XXX−XXX
pubs.acs.org/NanoLett

Tuning Magnetic Soliton Phase via Dimensional Confinement in Exfoliated 2D $Cr_{1/3}NbS_2$ Thin Flakes

Siwei Tang,[†,‡,§] Randy S. Fishman,[∥] Satoshi Okamoto,[∥] Jieyu Yi,[‡,§] Qiang Zou,[‡] Mingming Fu,[‡] An-Ping Li,[‡] David Mandrus,[§] and Zheng Gai*,[‡]

[†]State Key Laboratory of Powder Metallurgy, Central South University, Changsha 410083, China
[‡]Center for Nanophase Materials Sciences, Oak Ridge National Laboratory, Oak Ridge, Tennessee 37831, United States
[§]Department of Materials Science and Engineering, University of Tennessee, Knoxville, Tennessee 37996, United States
[∥]Materials Sciences and Technology Division, Oak Ridge National Laboratory, Oak Ridge, Tennessee 37831, United States

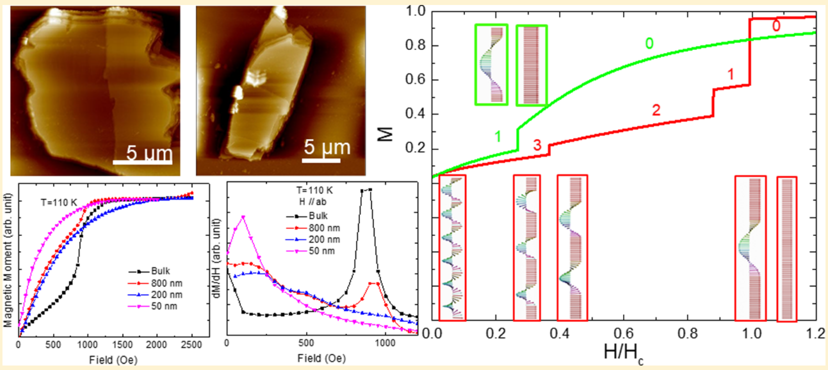

ABSTRACT: Thin flakes of $Cr_{1/3}NbS_2$ are fabricated successfully via microexfoliation techniques. Temperature-dependent and field-dependent magnetizations of thin flakes with various thicknesses are investigated. When the thickness of the flake is around several hundred nanometers, the softening and eventual disappearance of the bulk soliton peak is accompanied by the appearance of other magnetic peaks at lower magnetic fields. The emergence and annihilation of the soliton peaks are explained and simulated theoretically by the change in spin spiral number inside the soliton lattice due to dimensional confinement. Compared to the conventional magnetic states in nanoscale materials, the stability and thickness tunability of quantified spin spirals make $Cr_{1/3}NbS_2$ a potential candidate for spintronics nanodevices beyond Moore's law.

KEYWORDS: *2D materials, helimagnetism, soliton, ferromagnetism, dimensional confinement*

The competition between the exchange interaction and Dzyaloshinskii−Moriya (DM) interaction can result in chiral helimagnetism.[1,2] In helimagnetic materials, spins rotate in a specific crystal plane at a constant angle and then return to their original orientation over a distance called the pitch of the helix.[1−4] Examples of helimagnetic materials with spiral spin states include MnSi, $Fe_{1-x}Co_xSi$, FeGe, and $Cr_{1/3}NbS_2$. In the first three materials, the spin state transforms into a magnetic skyrmion lattice under magnetic field at particular temperatures.[5−7] $Cr_{1/3}NbS_2$ is formed by layers of transition metal dichalcogenide NbS_2 which are intercalated with the 3d magnetic element Cr, with lattice constants of a = 5.741 Å and c = 12.101 Å.[3,8,9] Cr atoms occupy octahedral sites within the van der Waals gaps of the NbS_2. The space group of $Cr_{1/3}NbS_2$ lacks an inversion center symmetry, similar to skyrmion materials. However, instead of forming a skyrmion lattice, $Cr_{1/3}NbS_2$ forms a unique magnetic soliton lattice when a magnetic field is applied perpendicular to the c-axis.[3,10−14] Above a critical magnetic field, the soliton lattice transforms into a ferromagnetic state.[9,15,16] In reduced dimensions, spin soliton confinement was recently observed in 1 μm wide grains of a $Cr_{1/3}NbS_2$ crystal, where discretized but robust electric transport effects were characterized.[17] Transport measurements were also performed on exfoliated thin flakes, where sharp and hysteretic resistance jumps were observed on flakes between 48 nm and 1 μm.[16] Those phenomena are believed to originate from the transitions between topological sectors with different numbers of magnetic solitons.[16,18] The magnetic properties of reduced dimension systems are obviously crucial to understand these phenomena, but were missing due to the limited magnetic signal of the thin flakes and small grains.

To reveal the thickness relationship between transitions of the soliton lattice and magnetism, we perform temperature-dependent and field-dependent magnetization measurements on thin flakes with various thicknesses. As the thickness of exfoliated flakes falls below about 10 times the cycloidal period 46 nm of $Cr_{1/3}NbS_2$, the bulklike soliton peak around 1000 Oe starts to change. That peak gradually disappears while other

Received: April 17, 2018
Published: May 2, 2018

DOI: 10.1021/acs.nanolett.8b01546
Nano Lett. XXXX, XXX, XXX−XXX

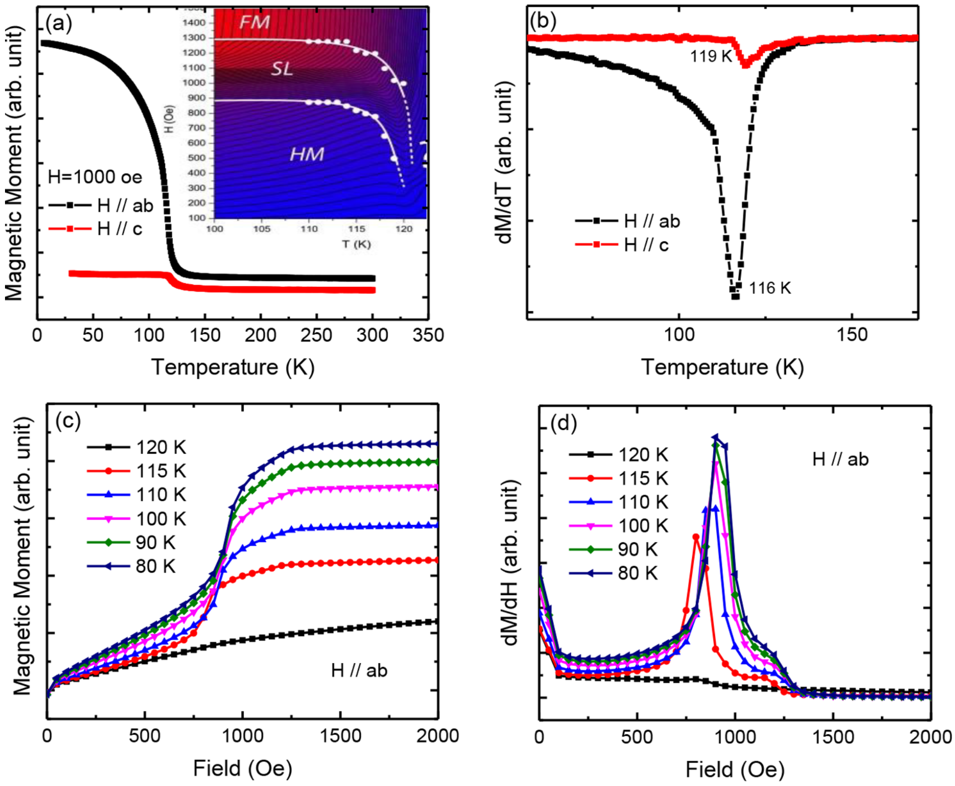

Figure 1. (a) Temperature-dependent magnetization of bulk $Cr_{1/3}NbS_2$ with magnetic field applied within the *ab*-plane (H // *ab*) or along the *c*-axis (H // *c*), H = 1000 Oe. Inset is a reproduction of the magnetic phase diagram from ref 12. FM, SL, and HM stand for ferromagnetic, soliton lattice, and helimagnetic phases. (b) First derivatives of the temperature-dependent magnetization with magnetic field within the *ab*-plane or along the *c*-axis. (c) Field-dependent magnetization of bulk $Cr_{1/3}NbS_2$, 80−120 K, H // *ab*. (d) First derivatives of the field-dependent magnetization dM/dH, 80−120 K. The soliton-ferromagnetism peak shifts to lower field at higher temperatures.

peaks appear at lower fields as the flakes become thinner. Theoretical calculations attribute the thickness-dependent magnetization to the change in the number of spin spirals inside the soliton lattice. When the thickness is thinner than the helical pitch, the magnetization becomes very robust against temperature and magnetic field. The robustness at nanometer length scales and the quantized spin spirals tunable by magnetic field and thickness make $Cr_{1/3}NbS_2$ a very promising candidate for spintronics beyond Moore's law, where conventional magnetic states become unstable as the size shrinks below a critical length.

Materials and Methods. The chemical vapor transport method was employed to grow single crystals of $Cr_{1/3}NbS_2$. A stoichiometric molar ratio of 1:3:6 of elements chromium, niobium, and sulfur powder was mixed in a glovebox and cold-pressed into dice. The dice were then placed in a vacuum sealed quartz tube and heated in an 800 °C oven to grow a polycrystalline powder. The temperature was slowly increased in case the quartz tube cannot sustain the pressure resulted from the rapid evaporation of sulfur. The powder was verified to be $Cr_{1/3}NbS_2$ by X-ray diffraction (XRD) analysis. Using iodine as the transport agent, the $Cr_{1/3}NbS_2$ powder was again sealed in a tube and heated in a tube furnace. Shiny flat platelike single crystals, as large as 5 × 5 × 1 mm in dimensions, were produced at the low-temperature end of the tube.

The structure and magnetic properties of each single crystal piece were first verified to be $Cr_{1/3}NbS_2$ before exfoliation. $Cr_{1/3}NbS_2$ flakes were fabricated by microexfoliation techniques using Scotch tape. Each individual flake was transferred to a clean silicon wafer for further characterization.

Thicknesses of the flakes were determined using ambient atomic force microscopy (AFM). Magnetic properties of the exfoliated $Cr_{1/3}NbS_2$ flakes on silicon wafer were characterized with a quantum design magnetic property measurement system (MPMS).[19] A single flake was laid flat on a Si wafer with a magnetic field applied perpendicular (H // *c*) or parallel (H // *ab*) to the flake.

Results and Discussion. Figure 1 shows the temperature-dependent magnetization and its derivative for two different directions of the applied magnetic field. Results are consistent with those reported previously.[12] Figure 1a,b is the results for the temperature-dependent magnetization (M-T) under 1000 Oe and the first derivative of the M-Ts. The latter show better details around the magnetic transition temperature (T_c). The magnetic transition is much broader and show kinks when H is applied within the *ab*-plane compared to H along *c* due to the existence of the soliton lattice for 900 Oe < H < 1300 Oe.[12] A magnetic phase diagram of the bulk material[12] is reproduced as an inset in Figure 1a, which shows the phase boundaries for the appearance of the soliton lattice from helimagnetism and its transformation into ferromagnetism at higher fields. Those complicated transitions are characterized by irregular slope changes in the field-dependent magnetization (M-H) for H // *ab* at temperatures below T_c. A set of such M-H curves are shown in Figure 1c. The first derivatives of the M-Hs, i.e., dM/dH, are shown in Figure 1d. The peak around 1000 Oe in Figure 1d is related to the soliton lattice. This peak shifts to lower field as the temperature approaches T_c and eventually disappears at 120 K, which is consistent with the magnetic phase diagram of the material.

DOI: 10.1021/acs.nanolett.8b01546
Nano Lett. XXXX, XXX, XXX−XXX

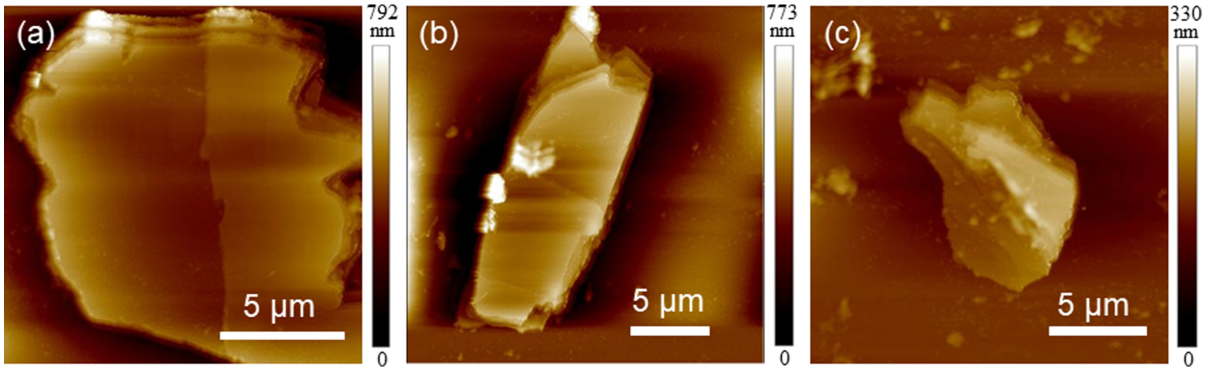

Figure 2. (a−c) AFM images of some exfoliated flakes of $Cr_{1/3}NbS_2$ with different sizes and thicknesses.

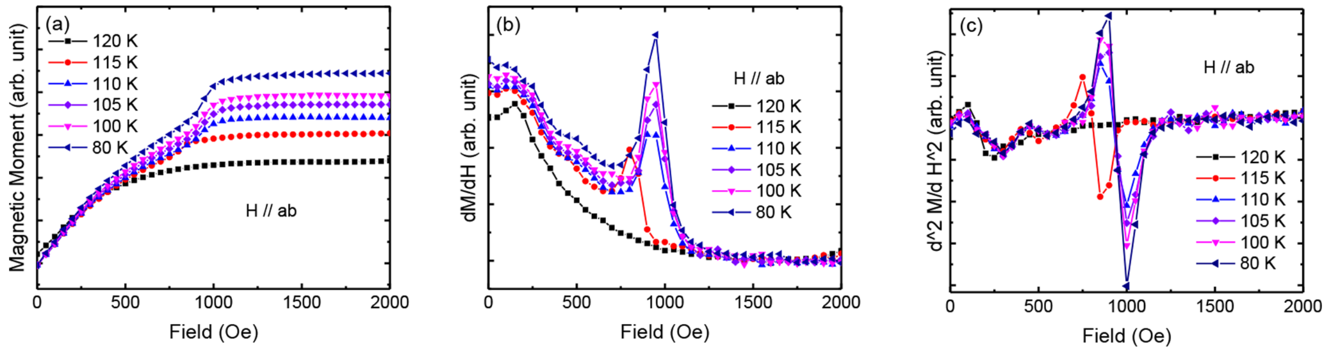

Figure 3. (a) Field-dependent magnetizations of a $Cr_{1/3}NbS_2$ flake (800 nm) with field applied within the *ab*-plane (H // *ab*) from 80 to 120 K. (b) First derivatives of the *M-Hs* in part a. (c) Second derivatives of *M-Hs* in part a. Note the appearance of new peaks at 250 and 500 Oe in addition to the bulklike 1000 Oe peak.

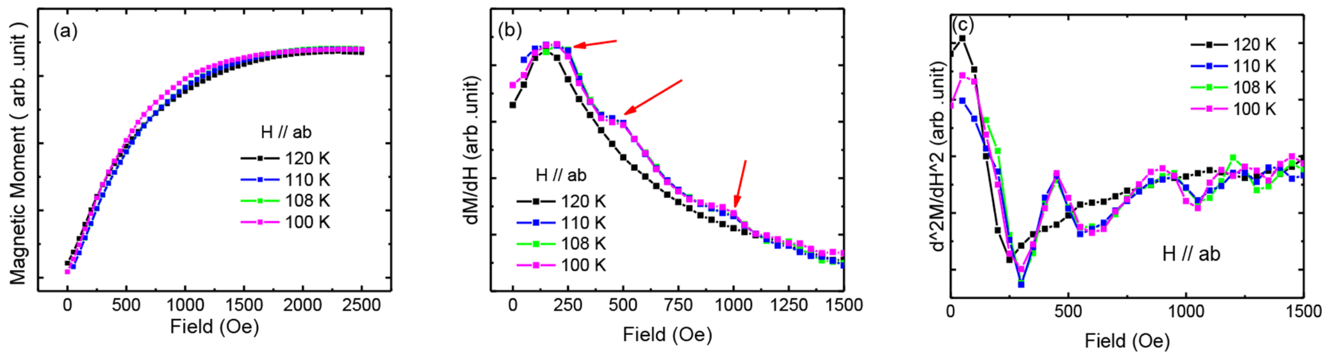

Figure 4. (a) Field-dependent magnetization of a $Cr_{1/3}NbS_2$ flake (200 nm) with magnetic field applied within the *ab*-plane (H // *ab*) from 100 to 120 K. (b) First derivatives of the *M-Hs* in part a. Note the downward-step feature is different than in thicker flakes. (c) Second derivatives of *M-Hs* in part a.

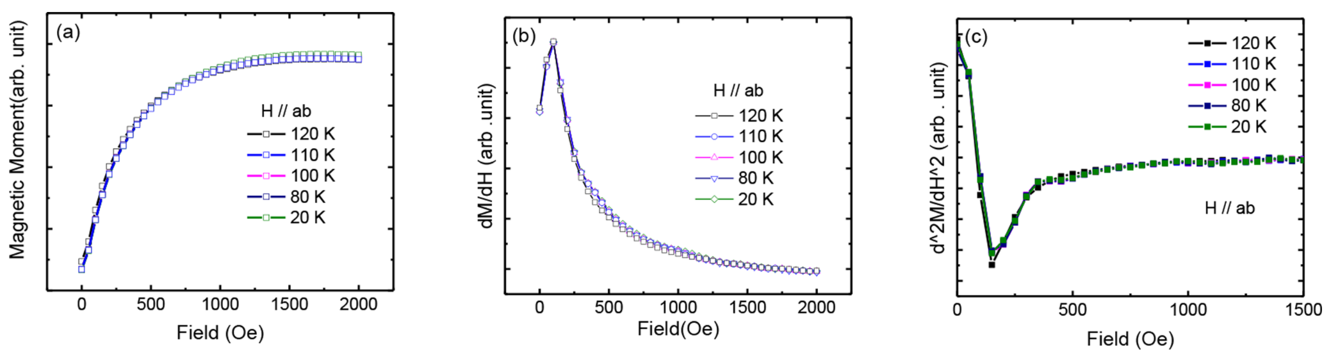

Figure 5. (a) Field-dependent magnetization of a $Cr_{1/3}NbS_2$ flake (50 nm) with magnetic field applied within the *ab*-plane (H // *ab*) from 20 to 120 K. (b) First derivatives of the *M-Hs* in part a. Note the disappearance of high field peaks. (c) Second derivatives of *M-Hs* in part a.

DOI: 10.1021/acs.nanolett.8b01546
Nano Lett. XXXX, XXX, XXX−XXX

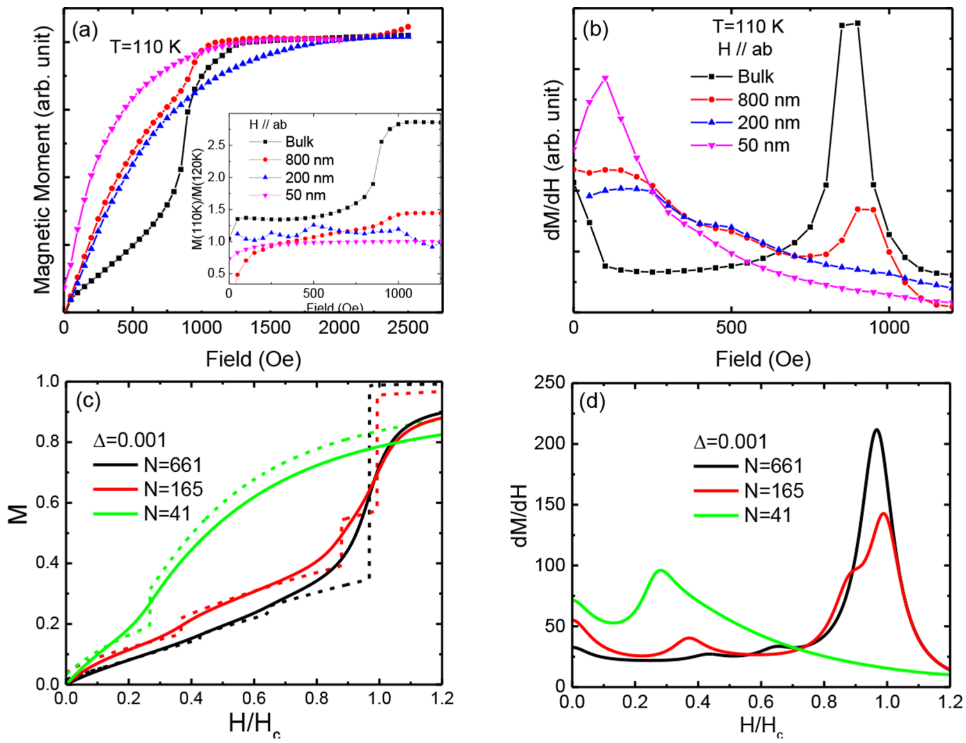

Figure 6. (a) Comparison of the M vs H curves of bulk and flakes at 110 K. Inset of part a directly compares M (110 K) normalized by M (120 K) for various thicknesses. (b) The first derivatives of the M-Hs in part a show the variation of main peak at different temperatures for bulk, 800, 200, and 50 nm flakes. (c) Simulation of in-plane field-dependent magnetization of flakes with thicknesses N = 661, 165, and 41 (corresponding to 800, 200, and 50 nm flakes) at Δ = 0.001. Δ is the width of the Lorentzian function used to smooth the numerical M vs H curves. Broken and solid lines are unsmoothed and smoothed M vs H curves, respectively. (d) Numerical results for the dM/dH curve using the theoretical model in ref 18.

After magnetic measurements on bulk $Cr_{1/3}NbS_2$ single crystals, they were exfoliated using Scotch tape. Figure 2a−c shows AFM images of several exfoliated flakes of $Cr_{1/3}NbS_2$, with the lateral size of the flakes dependent on the thickness. The cleavage surface is an *ab*-plane of the crystal structure. The surface is flat and smooth in both image contrast and detailed line profiles.

The crystal was exfoliated multiple times to get the desired thicknesses. Each exfoliate was followed by magnetic measurements using MPMS on single flake and thickness measurements using AFM. As the flake becomes thinner, the magnetization changes dramatically. Summarized in Figures 3, 4, and 5 are the magnetizations of three characteristic magnetic stages of the thin flakes corresponding to thicknesses of 800, 200, and 50 nm, respectively.

A flake with a thickness of 800 nm exhibits the same main feature as the bulk crystal, an isolated peak around 1000 Oe, but with a very different slope at lower magnetic field. As shown in Figure 3a, at low-field (below 500 Oe) magnetization develops new features, which make the change in slope around 1000 Oe less obvious than in the bulk. Consequently, the first derivatives of the M-Hs in Figure 3b show elevated dM/dH values and two small peaks at low fields (250 and 500 Oe). When the temperature is increased from 80 to 120 K, the 1000 Oe soliton-to-ferromagnetism peak shifts to lower fields with a decreased peak height, but the other two peaks remain at the same fields. The 500 and 1000 Oe peaks eventually disappear at 120 K, but the 250 Oe peak is still observable at 120 K. The above field-dependent evolution at different temperatures is more visible in the second derivative of the M-H as shown in Figure 3c. Both the 500 and 1000 Oe peaks shift with temperatures, although the 1000 Oe peaks shift more than the 500 Oe peaks; see later section for discussion.

Compared with the 800 nm flake, the M vs H curves of the 200 nm thick flake are almost monotonic and almost independent of temperature, as shown in Figure 4a for temperatures of 100, 108, 110, and 120 K. To better analyze the differences in the temperature-dependent magnetization, the first derivatives of those curves are plotted in Figure 4b. While the 120 K curves of the 800 and 200 nm samples (black curves in Figures 3b and 4b) are still very similar to each other (one peak at 250 Oe), the magnetic features observed in the 200 nm flake at temperatures below T_c are different, i.e., three robust downward stairlike peaks located at 250, 500, and 1000 Oe (Figure 4b), in stark contrast to the thicker samples where the 1000 Oe soliton lattice peak dominates. The 500 and 1000 Oe peaks disappear at 120 K, suggesting that the origin of these two peaks is the magnetic transition between 110 and 120 K, as in thicker samples. The above field and temperature evolution is more visible in the second derivative of the M-H in Figure 4c.

Magnetizations of the flake with a thickness of 50 nm, comparable to the pitch of the helix (46 nm in $Cr_{1/3}NbS_2$),[3,8,9] are shown in Figure 5. The field-dependent magnetization does not show any evidence of slope changes under high fields at all temperatures from 20 to 120 K (Figure 5a−c). For all temperatures, only one dM/dT peak appears in low fields, at about 100 Oe.

For direct comparison, the in-plane magnetizations and their first derivatives are plotted together for each flake at 110 K in Figure 6a,b. The inset of Figure 6a shows the quantitative relations among those curves by directly comparing the normalized magnetizations (normalized by their magnetization

DOI: 10.1021/acs.nanolett.8b01546
Nano Lett. XXXX, XXX, XXX−XXX

curves above the transition temperature). As the sample thickness decreases from bulk down to 50 nm, the magnetization curves gradually become smoother. The main soliton-to-ferromagnetism peak decreases in field and eventually disappears, while new subtransitions with much smaller peaks emerge at lower magnetic fields.

To understand the above behavior, the magnetization of thin flakes is simulated using the theoretical model described in ref 18, which proposed a theoretical phase diagram as a function of the film thickness N (dimensionless length scale) and external magnetic field H. Taking 46 nm for the cycloidal period of $Cr_{1/3}NbS_2$, and the lattice constant $c = 1.21$ nm, thicknesses of $N = 661$, 165, and 41 roughly simulate the film thicknesses 800, 200, and 50 nm, with spin spiral numbers n (or winding numbers) 17, 4, and 1, respectively.[3] Those parameters correspond to a zero-field spiral with wavelength $\Lambda \approx 40$, and ratio $D/J = -0.16$, where D is the Dzyaloshinskii−Moriya (DM) interaction, and J is the ferromagnetic exchange.[18,20] The observed slope changes in the magnetization of flakes with different thicknesses could be attributed to the change in the number of spin spirals inside the soliton lattice. When the number n of spin spirals changes, the M vs H curve exhibits a discontinuity. As shown as broken lines in Figure 6c, for the 50 nm flake ($N = 41$), the spiral only passes from an $n = 1$ to an $n = 0$ (ferromagnetic) state as the field H increases. However, for the 200 nm flake ($N = 165$), the spiral passes through states with $n = 4$, 3, 2, 1, and 0 as H increases. For the 800 nm flake ($N = 661$), the spiral passes through many more states. Note that, for $N = 165$, the $n = 1$ state located at $H/H_c = 0.993$ has a very narrow width and is invisible in this resolution. Similarly, for $N = 661$, states with $n = 13$ to 1 are condensed into a narrow region around $H/H_c = 0.968$. Under ideal conditions, the discontinuity of M vs H implies that dM/dH curves are sharply peaked at such critical fields H'. In reality, since the critical field H' depends on N, it is natural to anticipate that disorder effects, especially variation in the film thickness, will broaden such peaks in dM/dH. To simulate such disorder effects, we have convoluted numerical M vs H curves with a Lorentzian function with width $\Delta = 0.001$. The resulting M vs H curves are shown as solid lines in Figure 6c. The magnetic susceptibility dM/dH is then computed by numerically differentiating these smoothed M vs H curves as shown in Figure 6d.

One can see that the theoretical results capture the experimental characteristics fairly well; i.e., the peak position shifts from large H to small H as N decreases. However, the peak position shifts more slowly in the theory than in the experiment. This could be ascribed to additional disorders, which induce weak exchange links, inside experimental samples. By such disorders, the system could behave as an ensemble of weakly connected thinner systems. As the theoretical calculation does not include temperature, the reason for the preservation of the lowest field peak (250 Oe for 800 and 200 nm flakes, 100 Oe for the 50 nm flake) above T_c but not of the other peaks is still unknown. Further studies are necessary to understand this both experimentally and theoretically.

The ground state of $Cr_{1/3}NbS_2$ is a chiral helimagnetic structure due to the competition between ferromagnetism and the uniaxial DM interaction. When a magnetic field is applied within the ab-plane, some of the spins are aligned ferromagnetically within the chiral helimagnetic structure to create a soliton phase. Temperature has two effects on this process: First, it reduces the local ordered moment. Second, it reduces the spin−spin correlation length (short-range correlations can be finite even above the transition temperature). The influence of temperature increases close to the magnetic transition. Temperature has a weaker effect on the 500 Oe peak than on the 1000 Oe peak because the higher peak corresponds to the transition between low winding numbers. It is "softer" due to the larger number of aligned spins, which are suppressed near the transition temperature as discussed for the first effect above. Since the low-field peak corresponds to the transition between high winding numbers, it is "stiffer" due to the stronger DM interaction and is governed by the second effect. For the 50 nm flake, the thickness is almost the same as the spiral period of 46 nm. Therefore, the 100 Oe peak is very robust against temperature, for the same reasons discussed above.

To get a clearer physical picture of the magnetic soliton evolution, the spin configurations for two flakes are shown in Figure 7, 50 nm (green) and 200 nm (red). As a ground state, the chiral helimagnetic structure is stabilized at zero magnetic field (as shown in the spin configurations in the left side of Figure 7). With a small magnetic field applied along the ab-plane, part of the chiral helimagnetic structure is transformed into ferromagnetic arrays to form a chiral soliton lattice, which is composed of the leftover helimagnetic structure and the ferromagnetic spins. By further increasing the magnetic field to a critical value, the ferromagnetic arrays continue to expand, eventually resulting in a reduced number of spin spirals (magnetization jumps in Figure 7). When the magnetic field is large enough, all spins are reoriented toward the magnetic field (right side of Figure 7). The peaks in the first derivative of the field-dependent magnetization reflect this kind of transition, and the low-field peaks become more visible when the flake thickness is comparable to the spin spiral length.

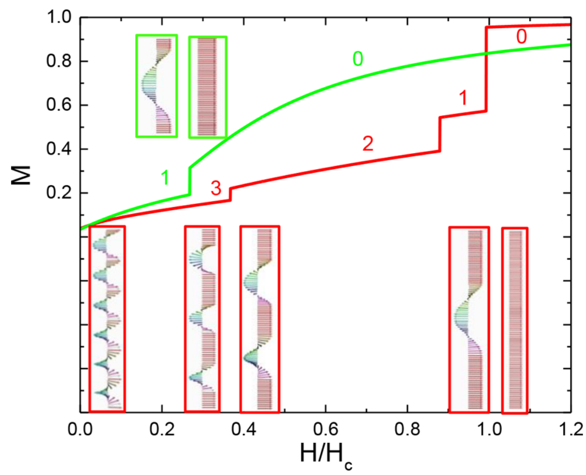

Figure 7. Schematic spin configurations for two flakes, green for $N = 41$ (or 50 nm), and red for $N = 165$ (or 200 nm), respectively.

Conclusion. The magnetic properties of exfoliated $Cr_{1/3}NbS_2$ thin flakes are compared with bulk properties. As the thickness of the exfoliated layer falls to one order higher than the cycloidal period 46 nm of $Cr_{1/3}NbS_2$, the magnetic behavior starts to change. As the flakes become thinner, the bulklike soliton peak around 1000 Oe gradually disappears, and new peaks appear. Theoretical calculations are employed to explain the observed thickness-dependent evolution of the magnetization. The novel emergence and annihilation of the

DOI: 10.1021/acs.nanolett.8b01546
Nano Lett. XXXX, XXX, XXX−XXX

soliton peaks are explained and simulated theoretically by the changes in the spin spiral number inside the soliton lattice due to dimensional confinement. By considering additional disorder parameters, the magnetization curves are reproduced successfully. The robustness of the nanometer-length-scale materials as well as the tunability of the spirals by magnetic field or thickness are all unexpected.

Moore's law, the principle that has powered the information-technology revolution since the 1960s, is nearing its end. Magnetic media faces a huge challenge to its further development: when shrunk below a critical size, the magnetic states in conventional magnetic hard disks can become unstable, resulting in data loss. We expect that the material and the physics discussed in this research may be useful in spintronics applications beyond Moore's law since the chiral spiral has a similar length scale but is even more robust than skyrmions. Moreover, the soliton lattice can be tuned by a magnetic field and temperature. Unlike a skyrmion, the soliton lattice is based on a chiral helimagnetic structure. Although the length of the soliton cannot be reduced further in the *c*-direction, its dimensions in the *ab*-plane can be reduced below the current storage density.

AUTHOR INFORMATION

Corresponding Author

*E-mail: gaiz@ornl.gov.

ORCID

Satoshi Okamoto: 0000-0002-0493-7568

An-Ping Li: 0000-0003-4400-7493

Zheng Gai: 0000-0002-6099-4559

Notes

The authors declare no competing financial interest.

ACKNOWLEDGMENTS

The experimental part of this research was conducted at the Center for Nanophase Materials Sciences, which is a DOE Office of Science User Facility. Part of the theoretical calculation (R.S.F.) was supported by LDRD project 7362. The research by S.O. is supported by the U.S. Department of Energy, Office of Science, Basic Energy Sciences, Materials Sciences and Engineering Division.

REFERENCES

(1) Mühlbauer, S.; Binz, B.; Jonietz, F.; Pfleiderer, C.; Rosch, A.; Neubauer, A.; Georgii, R.; Böni, P. Skyrmion Lattice in a Chiral Magnet. *Science* **2009**, *323* (5916), 915−919.

(2) Han, J. H.; Zang, J.; Yang, Z.; Park, J.; Nagaosa, N. Skyrmion Lattice in a Two-Dimensional Chiral Magnet. *Phys. Rev. B: Condens. Matter Mater. Phys.* **2010**, *82* (9), 94429.

(3) Togawa, Y.; Koyama, T.; Takayanagi, K.; Mori, S.; Kousaka, Y.; Akimitsu, J.; Nishihara, S.; Inoue, K.; Ovchinnikov, A. S.; Kishine, J. Chiral Magnetic Soliton Lattice on a Chiral Helimagnet. *Phys. Rev. Lett.* **2012**, *108* (10), 107202.

(4) Tang, S.; Kravchenko, I.; Yi, J.; Cao, G.; Howe, J.; Mandrus, D.; Gai, Z. Growth of Skyrmionic MnSi Nanowires on Si: Critical Importance of the SiO2 Layer. *Nano Res.* **2014**, *7* (12), 1788−1796.

(5) Jiang, W.; Upadhyaya, P.; Zhang, W.; Yu, G.; Jungfleisch, M. B.; Fradin, F. Y.; Pearson, J. E.; Tserkovnyak, Y.; Wang, K. L.; Heinonen, O.; et al. Blowing Magnetic Skyrmion Bubbles. *Science* **2015**, *349* (6245), 283−286.

(6) Yu, X. Z.; Kanazawa, N.; Onose, Y.; Kimoto, K.; Zhang, W. Z.; Ishiwata, S.; Matsui, Y.; Tokura, Y. Near Room-Temperature Formation of a Skyrmion Crystal in Thin-Films of the Helimagnet FeGe. *Nat. Mater.* **2011**, *10* (2), 106−109.

(7) Woo, S.; Litzius, K.; Krüger, B.; Im, M.; Caretta, L.; Richter, K.; Mann, M.; Krone, A.; Reeve, R. M.; Weigand, M.; et al. Observation of Room-Temperature Magnetic Skyrmions and Their Current-Driven Dynamics in Ultrathin Metallic Ferromagnets. *Nat. Mater.* **2016**, *15* (5), 501−507.

(8) Borisenko, E. B.; Berezin, V. A.; Kolesnikov, N. N.; Gartman, V. K. Structural and Magnetic Ordering of CrNb3S6 Single Crystals Grown by Gas Transport Method. *Phys. Solid State* **2017**, *59* (7), 1310−1313.

(9) Togawa, Y.; Kousaka, Y.; Nishihara, S.; Inoue, K.; Akimitsu, J.; Ovchinnikov, A. S.; Kishine, J. Interlayer Magnetoresistance due to Chiral Soliton Lattice Formation in Hexagonal Chiral Magnet CrNb3S6. *Phys. Rev. Lett.* **2013**, *111* (19), 197204.

(10) Slovokhotov, Y. N.; Zubavichus, Y. V.; Golub, A. S.; Akselrud, L. G.; Kulikov, L. M.; Semenov-Kobzar, A. A. XAFS Study of Local Atomic Environment in Well- and Ill-Ordered Transition Metal Sulfides MxTS2 (T = Mo, Nb, Ta) Derived from TS2 Intercalates. *Nucl. Instrum. Methods Phys. Res., Sect. A* **2001**, *470* (1−2), 295−301.

(11) Borisov, A. B.; Kishine, J.; Bostrem, I. G.; Ovchinnikov, A. S. Magnetic Soliton Transport over Topological Spin Texture in Chiral Helimagnet with Strong Easy-Plane Anisotropy. *Phys. Rev. B: Condens. Matter Mater. Phys.* **2009**, *79* (13), 134436.

(12) Ghimire, N. J.; McGuire, M. A.; Parker, D. S.; Sipos, B.; Tang, S.; Yan, J.-Q.; Sales, B. C.; Mandrus, D. Magnetic Phase Transition in Single Crystals of the Chiral Helimagnet Cr1/3NbS2. *Phys. Rev. B: Condens. Matter Mater. Phys.* **2013**, *87* (10), 104403.

(13) Braam, D.; Gomez, C.; Tezok, S.; de Mello, E. V. L.; Li, L.; Mandrus, D.; Kee, H.-Y.; Sonier, J. E. Magnetic Properties of the Helimagnet Cr1/3NbS2 Observed by μSR. *Phys. Rev. B: Condens. Matter Mater. Phys.* **2015**, *91* (14), 144407.

(14) Yoshizawa, D.; Kishine, J. I.; Kousaka, Y.; Togawa, Y.; Mito, M.; Akimitsu, J.; Inoue, K.; Hagiwara, M. Magnetic Resonance in the Chiral Helimagnet CrNb3S6. *Phys. Procedia* **2015**, *75*, 926−931.

(15) Kousaka, Y.; Nakao, Y.; Kishine, J.; Akita, M.; Inoue, K.; Akimitsu, J. Chiral Helimagnetism in T1/3NbS2 (T = Cr and Mn). *Nucl. Instrum. Methods Phys. Res., Sect. A* **2009**, *600* (1), 250−253.

(16) Wang, L.; Chepiga, N.; Ki, D.; Li, L.; Li, F.; Zhu, W.; Kato, Y.; Ovchinnikova, O. S.; Mila, F.; Martin, I.; et al. Controlling the Topological Sector of Magnetic Solitons in Exfoliated Cr1/3NbS2 Crystals. *Phys. Rev. Lett.* **2017**, *118* (25), 257203.

(17) Togawa, Y.; Koyama, T.; Nishimori, Y.; Matsumoto, Y.; McVitie, S.; McGrouther, D.; Stamps, R. L.; Kousaka, Y.; Akimitsu, J.; Nishihara, S.; et al. Magnetic Soliton Confinement and Discretization Effects Arising from Macroscopic Coherence in a Chiral Spin Soliton Lattice. *Phys. Rev. B: Condens. Matter Mater. Phys.* **2015**, *92* (22), 220412.

(18) Fishman, R. S.; Okamoto, S. Spiral Spin State with Open Boundary Conditions in a Magnetic Field. *Phys. Rev. B: Condens. Matter Mater. Phys.* **2017**, *96* (1), 14439.

(19) Tang, S.; Kravche, I.; Ward, T. Z.; Zou, Q.; Yi, J.; Ma, C.; Cao, G.; Li, A.; Mandrus, D.; Gai, Z. Dimensionality Effects in FeGe 2 Nanowires : Enhanced Anisotropic Magnetization and Anomalous Electrical Transport. *Sci. Rep.* **2017**, *7*, 7126.

(20) Chapman, B. J.; Bornstein, A. C.; Ghimire, N. J.; Mandrus, D.; Lee, M. Spin Structure of the Anisotropic Helimagnet Cr1/3NbS2 in a Magnetic Field. *Appl. Phys. Lett.* **2014**, *105* (7), 72405.

DOI: 10.1021/acs.nanolett.8b01546
Nano Lett. XXXX, XXX, XXX−XXX